Development of a new generation of high-resolution anatomical models for medical device evaluation: the Virtual Population 3.0

IOP Publishing | Institute of Physics and Engineering in Medicine Physics in Medicine and Biology

Phys. Med. Biol. **59** (2014) 5287–5303 doi:10.1088/0031-9155/59/18/5287

Development of a new generation of high-resolution anatomical models for medical device evaluation: the Virtual Population 3.0

Marie-Christine Gosselin[1,2], Esra Neufeld[1], Heidi Moser[1], Eveline Huber[1], Silvia Farcito[1], Livia Gerber[1], Maria Jedensjö[1], Isabel Hilber[1], Fabienne Di Gennaro[1], Bryn Lloyd[1], Emilio Cherubini[3], Dominik Szczerba[1], Wolfgang Kainz[4] and Niels Kuster[1,2]

[1] Foundation for Research on Information Technologies in Society (IT'IS), Zeughausstrasse 43, 8004 Zurich, Switzerland
[2] ETH Zurich, Zurich, Switzerland
[3] Schmid and Partner Engineering AG (SPEAG), Zurich, Switzerland
[4] FDA, Silver Spring, MD, USA

E-mail: gosselin@itis.ethz.ch

Received 3 December 2013, revised 13 February 2014
Accepted for publication 18 February 2014
Published 21 August 2014

Abstract

The Virtual Family computational whole-body anatomical human models were originally developed for electromagnetic (EM) exposure evaluations, in particular to study how absorption of radiofrequency radiation from external sources depends on anatomy. However, the models immediately garnered much broader interest and are now applied by over 300 research groups, many from medical applications research fields. In a first step, the Virtual Family was expanded to the Virtual Population to provide considerably broader population coverage with the inclusion of models of both sexes ranging in age from 5 to 84 years old. Although these models have proven to be invaluable for EM dosimetry, it became evident that significantly enhanced models are needed for reliable effectiveness and safety evaluations of diagnostic and therapeutic applications, including medical implants safety. This paper describes the research and development performed to obtain anatomical models that meet the requirements necessary for medical implant safety assessment applications. These include implementation of quality control procedures, re-segmentation at higher resolution, more-consistent tissue assignments, enhanced surface processing and numerous anatomical refinements. Several tools were developed

to enhance the functionality of the models, including discretization tools, posing tools to expand the posture space covered, and multiple morphing tools, e.g., to develop pathological models or variations of existing ones. A comprehensive tissue properties database was compiled to complement the library of models. The results are a set of anatomically independent, accurate, and detailed models with smooth, yet feature-rich and topologically conforming surfaces. The models are therefore suited for the creation of unstructured meshes, and the possible applications of the models are extended to a wider range of solvers and physics. The impact of these improvements is shown for the MRI exposure of an adult woman with an orthopedic spinal implant. Future developments include the functionalization of the models for specific physical and physiological modeling tasks.

Keywords: anatomical models, segmentation, human tissue parameters, high resolution

(Some figures may appear in colour only in the online journal)

1. Introduction

Numerical simulations are increasingly used to investigate the impact of external stressors on the human body, thereby complementing experimental studies. In the long term, the significance of numerical evaluations performed with computational human models can be expected to outweigh experimental studies. A simulation model must represent the interaction(s) under study by accurately adjusting the level of detail and relevant characteristics, which can range from the molecular or cellular level to tissue and whole-body anatomical representations. Historically, the latter are used routinely for dosimetric assessments of ionizing and non-ionizing radiation, but are also applied to other fields of research and applications, e.g., tissue mechanics, acoustics (in particular ultrasound), crash and blast investigations, orthopedic implant development and in the clothing industry. The complexity of the models has compounded significantly as a result of the increased availability and enhancement of computer resources over time. The 1950s saw the emergence of the first generation of models, namely generic or stylized models, consisting of geometrical shapes that only roughly represented the dimensions and outer shape of the body, and, depending on the application, of the organ(s) under investigation (Fisher and Snyder 1966, Billings and Yucker 1973, Cristy 1980, Tsui *et al* 1993). Voxel models based on data segmented from medical images were first developed in the 1980s (Zubal *et al* 1994, Jones 1997, Mason *et al* 2000, Gjonaj *et al* 2002, Petoussi-Henss *et al* 2002, Lee *et al* 2004, Dimbylow 2005, Sato *et al* 2007, Zhang *et al* 2007, Sato *et al* 2009, Christ *et al* 2010, Xu *et al* 2000) and are now commonly in use. Advanced models of the human body are currently represented by polygon meshes (Xu *et al* 2007, Christ *et al* 2010) or non-uniform rational B-spline (NURBS) surfaces (Lee *et al* 2007, 2008, Segars and Tsui 2009).

The complexity of the coupling of electromagnetic (EM) near-field sources with the human anatomy resulted in the early utilization of computational anatomical head models in the context of safety guidelines for compliance testing. The growing public concern over EM exposure led to the development of the Virtual Family (Christ *et al* 2010) by joint effort of the IT'IS Foundation and the United States Food and Drug Administration (FDA), funded by the Mobile Manufacturer Forum (Belgium), GSM Association (Switzerland), and SPEAG (Switzerland). It initially consisted of four anatomical models generated from the magnetic

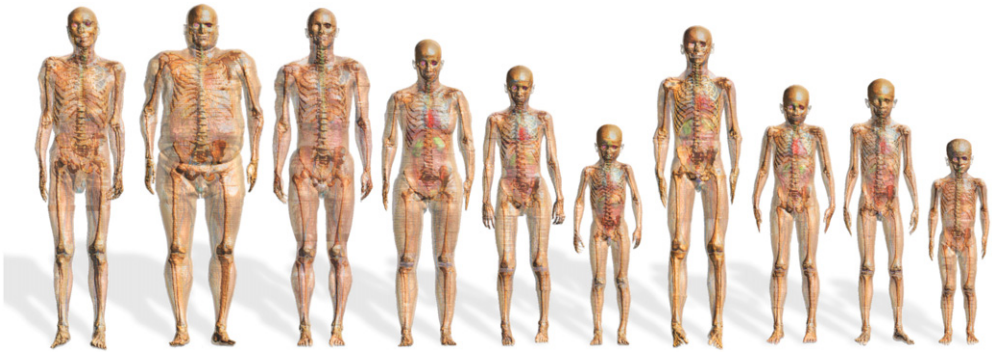

Figure 1. The complete Virtual Population representing humans (males and females) of different age groups and body shapes.

Table 1. Specifications of the Virtual Population models.

Name	Gender	Age (year)	Height (m)	Weight[a] (kg)	BMI (kg m^{-2})
Glenn	Male	84	1.73	65.0	21.7
Fats	Male	37	1.82	120.0	36.2
Duke	Male	34	1.77	72.4	23.1
Ella	Female	26	1.63	58.7	22.0
Louis	Male	14	1.69	50.4	17.7
Billie	Female	11	1.47	35.4	16.5
Eartha	Female	8	1.36	30.7	16.7
Dizzy	Male	8	1.40	26.0	13.4
Thelonious	Male	6	1.17	19.3	14.0
Roberta	Female	5	1.09	17.8	14.9
Nina	Female	3	0.92	13.9	16.4
Pregnant women (based on Ella; specifications refer to fetus)					
3rd month	Undefined	3 months		0.015	
7th month	Undefined	7 months		1.7	
9th month	Female	9 months		2.7	
Charlie	Female	8 weeks		4.3	

[a] The volume of given geometric structures is information that is intrinsic to each individual model but the weight is calculated based on the density of each tissue as in the IT'IS parameter database (Hasgall *et al* 2013).

resonance (MR) images of healthy volunteers: average-sized male and female adults and two children (a 6 year old boy and an 11 year old girl). These models were made available to the scientific community in 2008. To further extend the population coverage, the MR images of additional child volunteers (5 and 8 year old girls, and 5 and 14 year old boys) were segmented to create the Virtual Classroom. Increased coverage of anatomical variability is provided with obese (37 years old, 1.82 m, 120 kg) and elderly (84 years old, 1.73 m, 65 kg) male models, an 8 week old baby model, and three pregnant women models at gestational stages of 3, 7 and 9 months. Today, this widely used set of anatomical models is also known as the Virtual Population (ViP 1.0, figure 1, table 1).

The ViP 1.0 has been applied in a large variety of exposure studies, such as to mobile phones, wireless devices, MR imaging (MRI) scanners, home appliances, and safety and efficacy assessments of medical treatments, e.g., hyperthermia therapy or implant safety,

product development and optimization, and basic research, e.g., mechanistic investigations. However, while they have been employed in selected cases to the assessment of medical devices and therapies, e.g., safety of implants during MRI scanning or focused ultrasound ablation, the first generation of the Virtual Population suffers from limitations related to limited local detail and accuracy, unsuitable tissue surface quality, missing fine structures and insufficient fine structure continuity, as well as inconsistent segmentation across the different models. Furthermore, current devices often combine complex interactions from multiple domains of physics and physiology, sometimes in a coupled manner, which require models adapted to different solvers, e.g., a finite-element method (FEM) biomechanical solver. For example, the development and safety assessment of a cardiovascular implant requires modeling of computational fluid dynamics (CFD), EM compatibility (e.g., MR safety with regard to heating, forces and nerve stimulation), structural and tissue mechanics, treatment optimization and short- as well as long-term tissue adaptation aspects. To be useful, anatomical models must therefore be adapted to the needs of different numerical methods and physics/physiology modes. The FEM, for example, typically requires high-quality unstructured meshes.The generation of these meshes is significantly simplified when the underlying models feature topologically compatible interfaces between tissues, i.e., neighboring tissues share identical surface triangles at their interfaces and avoid self-intersection.

A significant research and development effort was necessary to overcome these restrictions. The various steps for the generation and the processing of the segmented data leading to polygon meshes, the associated tissue properties database and the tools developed to manipulate the meshes are presented and discussed herein. Finally, a case study is described in which the impact of the improvements of this new generation of models is shown in the context of exposure during a typical 1.5 T MRI scan of an adult woman with an orthopedic spinal implant.

2. Methods

2.1. Tools for model generation

The generation of each anatomical model includes the following steps (figure 3, figure 4):

(i) recruitment and whole-body scanning of a volunteer,
(ii) pre-processing of the MRI data,
(iii) segmentation of the medical image data to generate a label-field,
(iv) processing of the label-field to remove artifacts,
(v) extraction of the tissue surfaces,
(vi) processing of the surfaces.

2.1.1. Imaging and images pre-processing. The imaging of the volunteers was conducted in a 1.5 T whole-body scanner based on the MR protocol described in Christ *et al* (2010). The resolution of the resulting images was $0.5 \times 0.5 \times 1.0\,\text{mm}^3$ in the head and $0.9 \times 0.9 \times 2.0\,\text{mm}^3$ in the torso and the limbs. For the generation of the Virtual Population 3.0, the image data and label-fields generated for the first version of the models were up-sampled to $0.5 \times 0.5 \times 0.5\,\text{mm}^3$ by means of the Lanczos interpolation method (Duchon 1979) for the image data (figure 2) and voxeling of the original surface model for the generation of the up-sampled label-field.

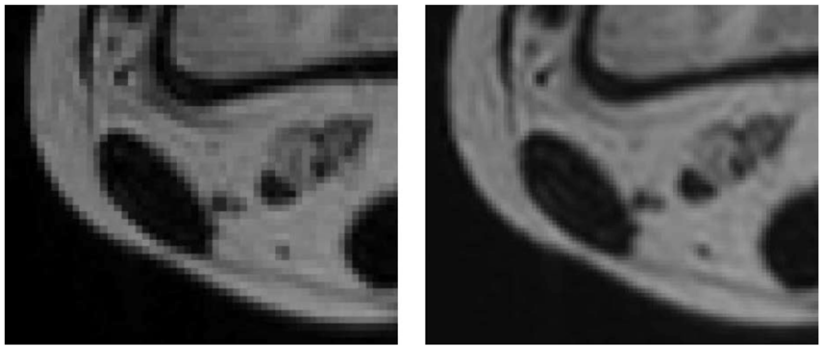

Figure 2. Resampling of an MRI scan of the leg from $0.9 \times 0.9 \times 2.0\,\text{mm}^3$ (left) to $0.5 \times 0.5 \times 0.5\,\text{mm}^3$ (right) by means of the Lanczos interpolation method. Although no additional information has been used to generate the higher-resolution image, some structures appear more clearly.

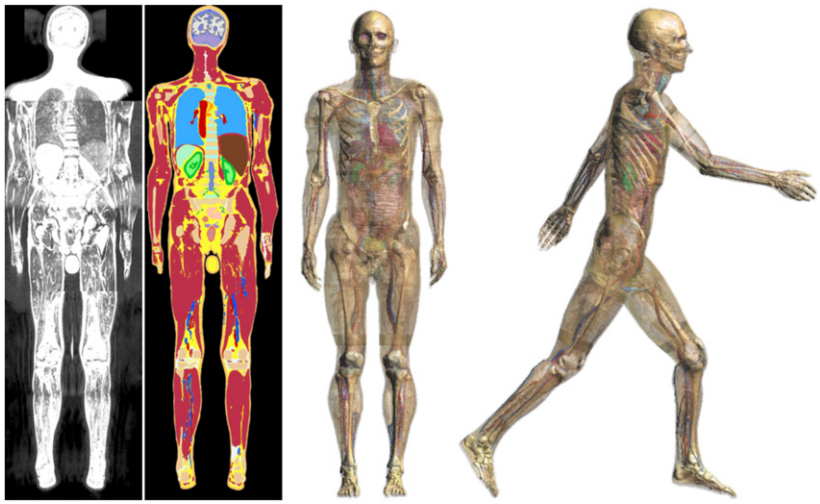

Figure 3. From left to right: raw MRI data, label-fields, surface model, and posed model (generated using the posing functionalities described in section 2.2.2).

2.1.2. Segmentation and label-field processing. The in-house software iSeg (Neufeld 2008) (ZMT Zurich MedTech AG, Switzerland) was used to identify the pixels belonging to different tissues (figure 3). iSeg offers a large number of image processing algorithms, such as Live Wire (Schenk *et al* 2000), Level Sets (Suri *et al* 2002), Region Growing (Hamerly and Elkan 2002), Fuzzy Connectedness (Udupa and Saha 2003), Interactive Watershed Transformation (Hahn and Peitgen 2003), etc. The segmentation tools range from highly interactive to fully automatic, and method-specific interaction paradigms are employed. iSeg also offers tools for topologically flexible interpolation that can be used to estimate tissue shapes between segmented layers to facilitate the model creation process (based on Raya and Udupa (1990) and Beucher (1998)). Routines for hole, gap and speckle removal, noise reduction, label-field smoothing (e.g., based on an implicit level-set approach), as well as adding skin layers are also available. All the functionalities of iSeg can be flexibly combined.

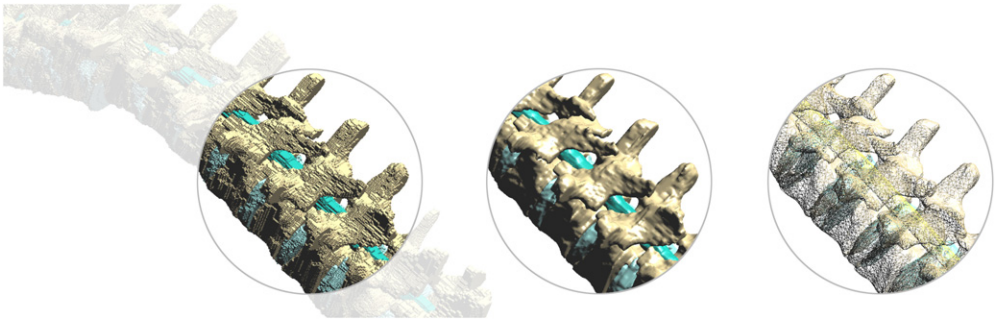

Figure 4. Surface extraction and processing (see section 2.1.3.). From left to right: results from surface extraction, feature- and volume-preserving smoothing, and surface simplification (here a triangle-count reduction by a factor of 40 is illustrated). These steps are required to generate the surface models from the label fields (cf figure 3).

2.1.3. Surface extraction and processing. Subsequently, topologically conformal (i.e., neighboring solids share common surface triangles), non (self-)intersecting triangle surfaces are extracted and processed. Conformal surfaces offer the advantages of avoidance of gaps between solids, simplification of the creation of high-quality tetrahedral meshes (e.g., for FEM modeling), and the guarantee that structures do not overlap. Intersections and self-intersections of the surfaces can invalidate the models in the discretization (meshing) step. The created surfaces should be smooth and the triangles not degenerated. The following steps are used in the implemented approach (figure 4): template-based tetrahedral mesh extraction, surface extraction, feature- and volume-preserving smoothing (Taubin 1995), and surface simplification. Self-intersections are avoided during smoothing by constraining adjacent tetrahedra to be positively oriented. Surface simplification avoids self-intersections by testing each edge collapse. The Delauney edge flips (Cheng and Dey 2007) used to improve the mesh quality also do not introduce self-intersections.

2.1.4. Quality control. Despite our very accurate knowledge of the human body, the segmentation of tissues and organs from MRI scans is subject to interpretation. For example, the locations of the transitions between the midbrain, pons, medulla oblongata and spinal cord are not strictly defined. Additionally, due to the resolution of the segmentation voxels and the 2-pixel-minimum criteria necessary for good surface reconstruction, structures thinner than 1 mm, such as thin membranes or blood vessels and nerves that are either of small diameter or too close to the surface, are ignored.

However, studies of the variability between models that are exposed to given stimuli (e.g., (non)-ionizing radiation or acoustic exposure) require those models to be segmented in a uniform/consistent manner. The segmentation or re-segmentation of the Virtual Population 3.0 models is based on detailed internal guidelines as well as a system of quality control that ensures that the segmentation is consistent, both within a model and amongst models.

Those guidelines list the necessary structures that must be segmented and provide a description of how individual tissues are defined. For example, a list of mandatory arteries and veins, which must be segmented regardless of the quality of the images, is provided—in the worst case, the data needed to add these structures can be drawn from anatomical atlases. Arteries and veins that would add to the anatomical accuracy of the segmentation are also listed, with the requirement that each of them is continuous. Similar concerns are stated for each segmented tissue.

Human errors or discrepancies in the interpretation of the tissue list and/or of the MR images are reduced by a system of quality control. Once a given stack of images has been segmented, the segmentation is assessed by a second team member for approval based on a checklist that includes all segmented tissues. After the stacks of images have been merged to generate a whole-body model, a similar quality control is also performed. Finally, a case-tracking system is used to gather comments from users, and those comments are then employed to remove errors and improve the models. The quality control procedure also includes the generation of a log file that describes the changes made in the newly released versions of each model.

2.2. Tools for model processing

2.2.1. Discretization. For numerical modeling, it is necessary to transform the models into discrete representations, i.e., voxels, tetrahedra, etc. Various discretization methods have been implemented in-house to create rectilinear (voxels, typically employed for finite-difference techniques) and tetrahedral (commonly employed in finite-element simulations) meshes from the anatomical models. The rectilinear, non-uniform gridder developed uses ray-tracing and robust intersection testing to create voxel models. Conformal sub-cells can be generated (Benkler *et al* 2008) to reduce the impact of stair-casing. To create high quality, body-fitted, multi-domain tetrahedron meshes, different meshing methods have been implemented: (i) Delauney refinement (Shewchuk 1998) followed by mesh optimization to remove slivers and improve mesh quality, and (ii) a cut-cell Octree-based method (Shephard and Georges 1991) with a smoothing step.

2.2.2. Posing. Posing functionalities are available to parameterize the posture of the models. Two approaches have been developed: (i) a volume-preserving, skeleton- and influence-region-based approach that allows real-time posing and is based on methods from the field of computer graphics (Cherubini *et al* 2008), and (ii) a physical-simulation-based approach, motivated by movement mechanics, that allows the user to prescribe the position of bones and performs a tissue mechanics simulation of the passive deformation of the soft tissues, resulting in more-realistic joint-region geometries. Approach (i) calculates deformation fields based on the influence regions and spherical blend skinning (Kavan and Žára 2005), which computes the interpolation of a set of transformations in the quaternion space. To ensure more-realistic deformation, the rigidity of the bone is considered and a simple spring correction is used on the non-rigid parts of the model. When approach (ii) is employed, the small strain, linear elastic approximation can be used for moderate posture changes. However, when strong warping is present, it is important to solve the full, nonlinear problem. The simulations can be computationally very demanding, as they require on the order of 100 000 000 tetrahedral elements. Dedicated high performance computing-enabled solvers, based on the PETSc framework (Balay *et al* 1997), have been developed for this purpose.

2.2.3. Morphing. To extend the population coverage, morphing functionality is provided that allows, e.g., the fat or muscle content to be increased or decreased to change the body-mass index (BMI) of the models while preserving realistic internal organ placement and tissue distributions. Two approaches are available: (i) a physical simulation-based approach similar to that developed for model posing and (ii) an interactive deformation field-based warping approach. Approach (i) is motivated by physiological fidelity and uses tissue mechanics simulations where the bones are treated as rigid, the soft tissues deform passively, and selected fatty or muscle tissues are assigned growing or shrinking forces. Anisotropic forces can be

used. In general, the small-strain, linear elastic approximation is valid, but the simulations are still computationally demanding. In approach (ii), a widget with a grid of control points that can be individually moved to define a deformation field that is then applied to the model is used. This approach has been used, e.g., to enlarge certain organs or to add breathing motion to the Virtual Population models. Multi-resolution rendering is used to provide real-time interactivity and visualization. It is also possible to pre-compute deformation fields for posing or morphing, e.g., with the physical simulation-based approach, and to interactively scale the displacement field to parameterize the degree of deformation.

2.2.4. Material assignment. Depending on the physics to be applied in the simulation, parameters—electric and magnetic conductivity, permittivity and permeability for EM simulations, or thermal conductivity, heat generation rate, heat transfer rate (perfusion) and heat capacity for thermal simulations—must be assigned to the tissues. Based on a comprehensive scientific literature review, a material parameter database (Hasgall *et al* 2013) that aims to provide the modeling community with average and range-of-variation values of EM and thermal properties as well as density and perfusion of biological tissues was compiled (http://www.itis.ethz.ch/database). The Virtual Population 3.0 is fully compatible with this database of tissue parameters, thanks to the consistent tissue naming assured by the quality control procedure described in section 2.1.4.

3. Results and discussion

3.1. Segmentation

The list of tissues identified in version 3.0 of the Virtual Population is more exhaustive than that of version 1.0 (see table 2), and most of the additional tissues have now been segmented as a result of the resampling described in section 2.1.1, which provides more pixels within the structures. Limitations pointed out in the original Virtual Family publication (Christ *et al* 2010) and issues reported by the scientific community are, for the most part, resolved in version 3.0 of the models:

- No blood vessels smaller than 2 mm were segmented in version 1.0; version 3.0 includes blood vessels as small as 1 mm in diameter. All blood vessels are continuous.
- The spinal cord and optical nerve were segmented in version 1.0; version 3.0 also includes initial sections of the spinal nerves (about 2 cm) as well as the sciatic and tibial nerves.
- The pancreas was reconstructed only in the male adult in version 1.0; it is now segmented in all models.
- The salivary glands are now segmented.
- The lumen of the small intestine is added using a wall thickness of 3.5 mm (Schmidt 2005).
- The stomach and the gall bladder were hardly distinguishable from their lumens on the MRI scans; these are now segmented with fixed thicknesses of 6 mm (Schmidt 2005) and 1.5 mm (Spurway *et al* 2004), respectively.
- Bone marrow (red) was segmented for the male models of the Virtual Family 1.0. In version 3.0, three layers of bones are distinguished, cortical bone, cancellous bone and bone marrow. The conversion of red marrow to yellow marrow in humans is age-dependent but differs from bone to bone. This age-dependent transformation is estimated by segmenting the marrow as red for models younger than 20 years of age and yellow for older models.
- The thymus is usually large at birth and increases in size with age until puberty. After puberty, the thymus degenerates and is transformed into fatty tissues. It is, thus, segmented only in children.

Table 2. Tissues segmented in the Virtual Population 3.0 models.

• In all models:			
– Adrenal gland	– Esophagus	– Larynx	– Spinal cord
– Air internal	– Esophagus (lumen)	– Liver	– Spleen
– Arteries	– Eye (lens)	– Lung	– Stomach
– Bladder	– Eye (sclera)	– Lymph node	– Stomach (lumen)
– Blood vessel	– Eye (vitreous humor)	– Medulla oblongata	– Teeth
– Bone	– Fat	– Meniscus	– Tendon
– Brain (grey matter)	– Gallbladder	– Midbrain	– Thalamus
– Brain (white matter)	– Gallbladder bile	– Mucosa	– Thymus
– Bronchi	– Heart (lumen)	– Muscle	– Thyroid gland
– Bronchi (lumen)	– Heart (muscle)	– Nerve	– Tongue
– Cartilage	– Hippocampus	– Pancreas	– Trachea
– Cerebellum	– Hypophysis	– Pineal body	– Trachea (lumen)
– Cerebrospinal fluid	– Hypothalamus	– Pons	– Ureter
– Commissura anterior	– Intervertebral disc	– Salivary gland	– Urethra
– Commissura posterior	– Kidney (cortex)	– SAT	– Urine
– Cornea	– Kidney (medulla)	– Skin	– Veins
– Corpus callosum	– Large intestine	– Small intestine	
– Diaphragm	– Large intestine (lumen)	– Small intestine (lumen)	
• Bones[a]:			
– Calcaneus	– Mandible		– Trapezium
– Capitatum	– Metacarpus (I to V)	– Pisiforme	– Trapezoideum
– Clavicle	– Os sacrum and coccyx	– Radius	– Triquetrum
– Femur	– Patella	– Rib	– Ulna
– Fibula	– Pelvis	– Scaphoideum	– Vertebra C1 to C7
– Foot	– Phalanx distalis (I to V)	– Scapula	– Vertebra L1 to L5
– Hamatum	– Phalanx media (II to V)	– Skull	– Vertebra T1 to T12
– Humerus	– Phalanx proximalis (I to V)	– Sternum	
– Hyoid		– Talus	
– Lunatum		– Tibia	
• In females only:			
– Breast tissue	– Oviduct	– Vagina	
– Ovary	– Uterus		
• In males only:			
– Ductus deferens	– Penis	– Seminal vesicle	
– Epididymis	– Prostate	– Testes	
• In adults only:			
– Yellow bone marrow			
• In children and adolescents only:			
– Red bone marrow	– Some bones are cartilage	– Two rows of teeth (milk and permanent)	
– Thymus			

[a] All bones are constituted of cortical bone, and some also include cancellous bone and/or bone marrow.

- In version 1.0, the stacks of images were segmented independently, the surfaces were extracted for each stack separately, and those parts of the model were aligned and merged as a final step, which led to discontinuous tissues. In version 3.0, the alignment and merging was performed with the label-fields, and the overlapping regions where the stacks of images are merged are corrected to obtain smooth transitions of the outside surface as well as the inner tissues prior to surface extraction.

The continuity and improved smoothness of the tissues and organs identified is a direct consequence of the higher resolution of the segmentation as well as the new algorithms used for the generation and processing of the surfaces. In addition to an extended list of well-defined segmented tissues, the strict internal quality control procedure developed and implemented by the segmentation group leads to very consistent segmentation, which will, in turn, lead to more-relevant variability studies.

3.2. Model generation

While the image segmentation approach has remained largely unchanged from that used to generate the first Virtual Family models, the implicit label-field smoothing step is new and facilitates removal of unwanted features. Also, the surface extraction and processing have been updated: previously, the surface extraction, simplification, and smoothing routines from the Amira software (Stalling *et al* 2005) were used. However, while Amira can produce conformal interfaces, the surface processing results in self-intersecting surfaces and, occasionally, poor element quality. In addition, the processing is very time consuming and cannot cope with whole-body high-resolution anatomical models. Therefore, the processing had to be performed piece-wise, and the resulting solid sections had to be merged. The merging step introduces multiple problematic issues such as wrongly oriented triangles, gaps, or overlapping regions. The new surface extraction and processing routines avoid these problems and produce high-quality surfaces, possibly however, at the expense of limiting the degree of achievable simplification, which results in a larger number of triangles.

3.3. Model processing

Discretization functionalities are required to make the models useable for numerical modeling. The specifications for models suitable for numerical methods requiring only rectilinear grids and voxels are relatively moderate, i.e., robust intersection detection must be possible, and there should be no inverted elements or other model aspects such as non-conformal surfaces that result in wrongly labeled voxels or holes. The requirements for unstructured mesh generation are far more demanding, including the need for good-quality triangle surfaces, i.e., non-degenerate triangles, smooth surface patches and non-manifold edges, as well as closed, conforming surfaces without self-intersections, which obviate the need for complicated remeshing. Even when these requirements are mostly satisfied, meshing complex and often noisy anatomical models remains a challenging task. The Delaunay refinement meshing approach is quite sensitive to the quality of the extracted surfaces. In comparison, the cut-cell Octree method is more tolerant. However, it re-generates the surfaces completely, which can sometimes remove desired features.

Having the capability to generate unstructured meshes as well as voxels allows the range of solvers that can be used and physical effects that can be simulated with the anatomical models to be considerably extended. In addition to the traditional applications in EM dosimetry, the Virtual Population 3.0 models and their predecessors have also been used for instance in biomechanical simulations, acoustic modeling, blood flow simulations (Neufeld *et al* 2013a, 2013b, Kyriakou *et al* 2012).

The posing and morphing functionalities allow the population and situation coverage by the Virtual Population 3.0 to be extended. The simulation-based approaches, while being computationally very demanding and not interactive, produce more-realistic results, e.g., variation of BMI by up to 50% and more-realistic joint geometries. The interactive warping has been used to change body and organ shapes, but also image-based information has been

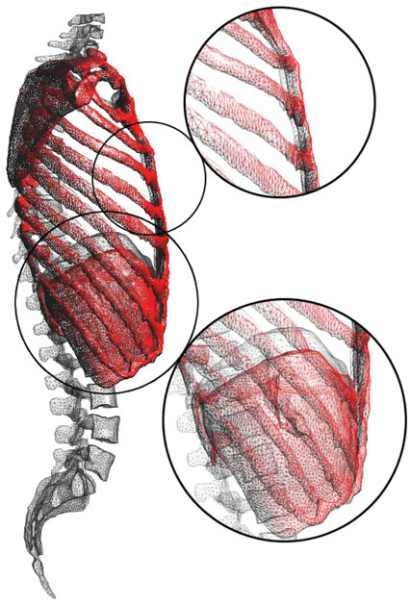

Figure 5. Triangular mesh of Duke's ribcage, spinal column, and liver at a state of complete inhalation (red) and complete exhalation (gray). The deformation of the model was facilitated through 4D MRI data acquired during the respiratory cycle of a healthy volunteer (von Siebenthal *et al* 2007). The image data were processed to extract the vectorial displacement fields and registered to a modified version of the original Duke 3.0 model, which was scaled to match the body type of the volunteer. The displacements were applied to that model with SEMCAD X at 14 stages throughout the breathing cycle.

used to mimic a complete breathing cycle, including the rib movement, internal organ shifting and lung volume changes (see figure 5).

3.4. The Virtual Population

The four models of the Virtual Family (Duke, Ella, Billie and Thelonious), the four models of the Virtual Classroom (Louis, Eartha, Dizzy and Roberta), the obese male, Fats, and the elderly male, Glenn, were all generated from MRI scans of volunteers recruited by or for the IT'IS Foundation (table 1). Figure 6 illustrates how these models compare to statistical data of the German population (Juergens 2004). Further models have been generated by morphing to extend the population coverage with a decreased effort compared to the segmentation of a whole body, which requires about one man-year, depending on the size of the model and the quality of the MRI data.

A 3 year old girl, Nina, was generated by morphing the 5 year old Roberta with the field-based warping morphing tool described in section 2.2.3. Scaling of the head was applied based on statistics from Snyder *et al* (1975), followed by anisotropic morphing of the body based on data from De Onis *et al* (2006) and Sempé *et al* (1979). Pregnant women models at three gestational stages presented in Christ *et al* (2012) are included in the Virtual Population. An 8 week old baby girl, Charlie, is also included and has been adapted from the voxel baby developed by the Helmholtz Zentrum München (previously known as Gesellschaft für Strahlenforschung, or GSF) (Petoussi-Henss *et al* 2002) to be consistent with the segmentation guidelines. Finally, a combination of the two morphing tools described above was used to generate ten additional adult models of various BMIs based on Duke, Ella and Fats.

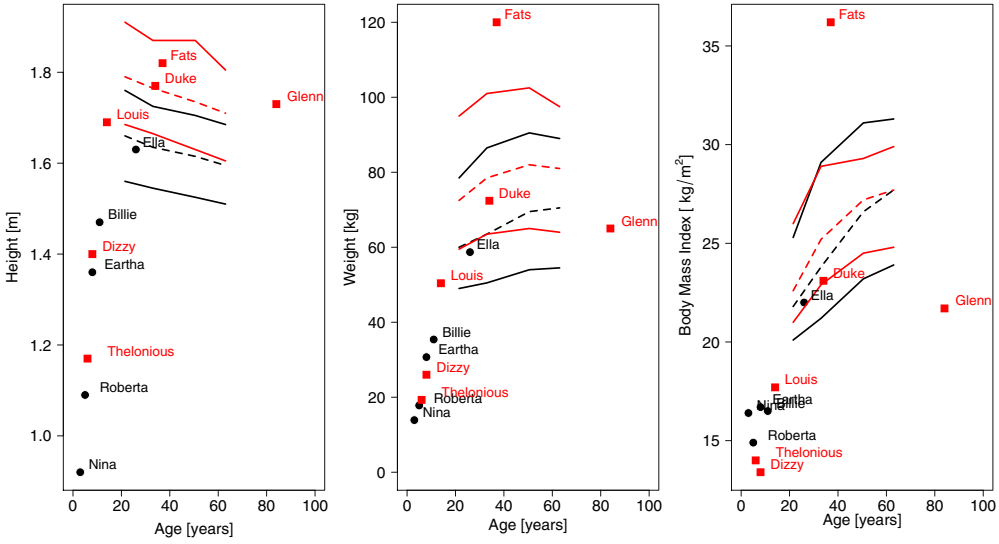

Figure 6. Comparison of height, weight and BMI from the Virtual Population models with age-dependent statistical data of the German population (Juergens 2004). Red and squares are used for males, black and circles for females.

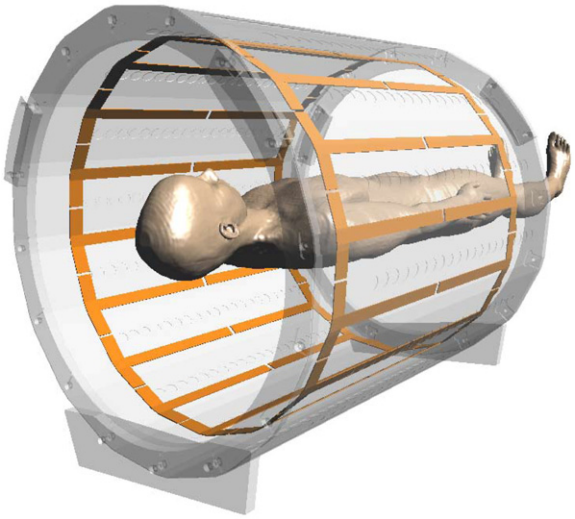

Figure 7. Ella version 3.0 in cardiovascular imaging position in the birdcage coil MITS1.5.

4. Case study

To see the impact of the differences between versions 1.0 and 3.0 of the models, the finite-difference time-domain simulation platform SEMCAD X was used to run an application example. Figure 7 shows the simulation setup of cardiovascular MRI scans at 1.5 T applied to the model of the adult woman Ella with a spinal implant. The simulation was run according to the specifications described in Cabot *et al* (2013). The 16-rung birdcage coil (length 750 mm,

Figure 8. Vertebrae, intervertebral discs and spinal column of Ella in versions 1.0 and 3.0 (left). Generic thoracolumbar stabilization implant inserted in the L2, L3 and L4 vertebrae of Ella versions 1.0 and 3.0 (right).

diameter 650 mm) is a numerical representation of the MITS1.5 (Medical Implant Test System, Zurich Med Tech, Switzerland). It was tuned with lumped elements placed at the end rings between the rungs to match previously performed measurements (Cabot *et al* 2013). Due to the high resolution required by the implant and the large simulation domain required by the birdcage coil, the computation was performed in two steps: the fields in the birdcage coil were computed from the empty coil, and those fields were used to simulate the exposure in the body based on Huygens' principle (Benkler *et al* 2009). For the latter, the model was discretized with a resolution of 2 mm in the body and 0.5 mm in the implant, leading to 135 Mcells in the computational domain. The assignment of the dielectric tissue properties at 64 MHz was done according to the material database (see section 2.2.4), which includes work presented in Gabriel *et al* (1996), and all metallic parts of the coil and the implant were treated as perfect electrical conductors.

A generic thoracolumbar stabilization implant was modeled and placed realistically between the L2 and L4 vertebrae (figure 8). Positioning of the implant was performed first in version 3.0 of the model, then copied to version 1.0, with slight adjustment to the positions of the screws, leading to very similar exposure configurations for both versions of the model. Positioning all the individual components of the implant, i.e. the six screws, two rods and four parts of the bridge, in the version 1.0 model only, would have been very inaccurate and would have led to an unrealistic, possibly unusable, setup. This accuracy of positioning will be even more critical for flexible cardiac or neural implants threaded through thin tissues or along a very specific path.

Figure 9 shows the local SAR distribution in the torso of Ella for both versions of the model. The more realistic shape of the lungs, liver and kidneys can clearly be recognized from the SAR distribution of version 3.0. The higher level of detail in the version 3.0 model also leads to a better appreciation of the exposure in the vertebrae, where the layer of cortical/cancellous

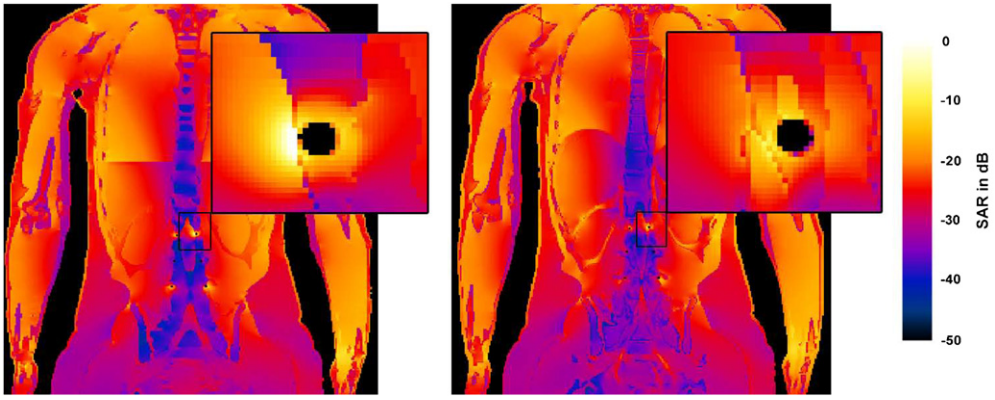

Figure 9. Comparison of the local SAR distribution in Ella versions 1.0 (left) and 3.0 (right) from the exposure to a 1.5 T MRI birdcage coil. 0 dB corresponds to a local SAR of 1000 W kg^{-1} for operation at first level control mode, i.e. for a whole-body SAR of 4 W kg^{-1}.

bones can clearly be distinguished; by comparison, version 1.0 includes only one type of bone in the vertebrae, the cortical bone. The local distribution around one screw is displayed in more detail, demonstrating the importance of accuracy in positioning the implant, which here leads to a local SAR one order of magnitude higher in version 1.0 than in version 3.0, due to an unrealistic contact of the screw with the CSF. It also shows the more-complex representation of the tissue distribution around the screw that results from the additional bone layer, as well as the newly segmented spinal nerves.

5. Conclusions

The Virtual Population 3.0 (ViP 3.0) is a set of computational models of independent anatomies including both sexes, with ages spanning from fetus to 84 years old and adult BMIs ranging from 21.7 to 36.2. The models have been greatly enhanced and refined to make them suitable for medical applications involving a broad range of solvers and multi-physics couplings. In parallel, a database that provides access to various dielectric and thermal tissue parameters, as well as perfusion and density information from the literature has been created. The new generation of human models, ViP 3.0, includes re-segmentation at higher resolution, more-consistent tissue assignment, several anatomical refinements, and offers the advantage of being based on truly independent anatomies. Functionalization of the models, e.g., by integration of inhomogeneous property maps or dynamic behavior (e.g., blood flow or neuron models), will be the next step.

Acknowledgments

The authors would like to thank the research group of Professor Klaas Prüssmann (ETH Zurich, Switzerland) for performing the MR imaging of the volunteer for the generation of the model Glenn, and Siemens Healthcare (Erlangen, Germany) for the imaging of the obese male volunteer corresponding to Fats. The development of the 3 year old girl model has received funding from the European Union's Seventh Framework Programm ([FP7/2007-2013]) under grant agreement no. 282891. The authors would like to thank the team of biologists at THESS

(Thessaloniki, Greece) for their valuable segmentation work and the independent review of the models. The authors would also like to thank Ludwig Tay for the realization of the generic implant model. Marie-Christine Gosselin is a NSERC (Natural Sciences and Engineering Research Council of Canada) grant holder.

Disclaimer

The mention of commercial products, their sources or their use in connection with material reported herein is not to be construed as either an actual or implied endorsement of such products by the Department of Health and Human Services.

References

Balay S, Gropp W D, McInnes L C and Smith B F 1997 Efficient management of parallelism in object oriented numerical software libraries *Modern Software Tools in Scientific Computing* ed E Arge, A M Bruaset and H P Langtangen (Basel: Birkhäuser) pp 163–202

Benkler S, Chavannes N and Kuster N 2008 Mastering conformal meshing for complex CAD-based C-FDTD simulations *IEEE Antennas Propag. Mag.* **50** 45–57

Benkler S, Chavannes N and Kuster N 2009 New powerful FDTD source based on Huygens surface: highly complex EM simulations performed on an ordinary PC *Abstract Collection of BioEM 2009 Davos: the Joint Meeting of the Bioelectromagnetics Society and the European BioElectromagnetics Association (Davos, Switzerland 14–19 June)* (Poster presentation P-262 in Poster session 2: Theoretical and Practical Modeling (June 16)) pp 736–7

Beucher S 1998 Sets, partitions and functions interpolations *Int. Symp. on Mathematical Morphology and its Applications to Image and Signal Processing IV* pp 3–5

Billings M and Yucker W 1973 *The Computerized Anatomical Man (CAM) Model* NASA CR-134043 (Houston, TX: Johnson Space Center)

Cabot E, Lloyd T, Christ A, Kainz W, Douglas M, Stenzel G, Wedan S and Kuster N 2013 Evaluation of the RF heating of a generic deep brain stimulator exposed in 1.5 T magnetic resonance scanners *Bioelectromagnetics* **34** 104–13

Cheng S-W and Dey T K 2007 Delaunay edge flips in dense surface triangulations arXiv:0712.1959

Cherubini E, Chavannes N and Kuster N 2008 Realistic skeleton based deformation of high-resolution anatomical human models for electromagnetic simulation *BEMS 2008: Abstracts of the 30th Annu. Meeting of the Bioelectromagnetics Society (San Diego, CA, USA, 9–12 June)* pp 505–7 (Poster Presentation P-149 in Poster Session: Theoretical and Practical Modeling) (10 June))

Christ A, Guldimann R, Bühlmann B, Zefferer M, Bakker J F, van Rhoon G C and Kuster N 2012 Exposure of the human body to professional and domestic induction cooktops compared to the basic restrictions *Bioelectromagnetics* **33** 695–705

Christ A *et al* 2010 The Virtual Family—development of surface-based anatomical models of two adults and two children for dosimetric simulations *Phys. Med. Biol.* **55** N23–N38

Cristy M 1980 Mathematical phantoms representing children of various ages for use in estimates of internal dose *Oak Ridge National Laboratory Technical Report ORNL* (Oak Ridge, TN: ORNL)

De Onis M *et al* 2006 *WHO Child Growth Standards: Length/Height-For-Age, Weight-For-Age, Weight-For-Length, Weight-For-Height and Body Mass Index-For-Age: Methods and Development* (Geneva: WHO)

Dimbylow P 2005 Development of the female voxel phantom, NAOMI, and its application to calculations of induced current densities and electric fields from applied low frequency magnetic and electric fields *Phys. Med. Biol.* **50** 1047–70

Duchon C E 1979 Lanczos filtering in one and two dimensions *J. Appl. Meteorol.* **18** 1016–22

Fisher H Jr and Snyder W 1966 Variation of dose delivered by 137Cs as a function of body size from infancy to adulthood *Oak Ridge National Laboratory Report ORNL-4007* (Oak Ridge, TN: ORNL) pp 221–8

Gabriel S, Lau R W and Gabriel C 1996 The dielectric properties of biological tissues: III. Parametric models for the dielectric spectrum of tissues *Phys. Med. Biol.* **41** 2271–93

Gjonaj E, Bartsch M, Clemens M, Schupp S and Weiland T 2002 High-resolution human anatomy models for advanced electromagnetic field computations *IEEE Trans. Magn.* **38** 357–60

Hahn H K and Peitgen H-O 2003 IWT-interactive watershed transform: a hierarchical method for efficient interactive and automated segmentation of multidimensional gray-scale images *Medical Imaging 2003: Proc. Conf. of Int. Soc. for Optics and Photonics* pp 643–53

Hamerly G and Elkan C 2002 Alternatives to the k-means algorithm that find better clusterings *Proc. 11th ACM Int. Conf. on Information and Knowledge Management* pp 600–7

Hasgall P, Neufeld E, Gosselin M-C, Klingenböck A and Kuster N 2013 IT'IS database for thermal and electromagnetic parameters of biological tissues Version 2.4 www.itis.ethz.ch/database

Jones D 1997 A realistic anthropomorphic phantom for calculating organ doses arising from external photon irradiation *Radiat. Prot. Dosim.* **72** 21–29

Juergens J W 2004 Erhebung anthropometrischer Masse zur Aktualisierung der din 33 402—teil 2 (Survey of anthropometric dimensions for the revision of din 33 402—part 2) *Technical Report* (Schriftenreiheder Bundesanstalt für Arbeitsschutz und Arbeitsmedizin)

Kavan L and Žára J 2005 Spherical blend skinning: a real-time deformation of articulated models *Proc. 2005 ACM Symp. on Interactive 3D Graphics and Games* pp 9–16

Kyriakou A, Neufeld E, Szczerba D, Kainz W, Lüchinger R, Kozerke S, McGregor R and Kuster N 2012 Patient-specific simulations and measurements of the magneto-hemodynamic effect in human primary vessels *Physiol. Meas.* **33** 117–30

Lee C, Lee J and Lee C 2004 Korean adult male voxel model Korman segmented from magnetic resonance images *Med. Phys.* **31** 1017–22

Lee C, Lodwick D, Hasenauer D, Williams J L, Lee C and Bolch W E 2007 Hybrid computational phantoms of the male and female newborn patient: NURBS-based whole-body models *Phys. Med. Biol.* **52** 3309–33

Lee C, Lodwick D, Williams J L and Bolch W E 2008 Hybrid computational phantoms of the 15-year male and female adolescent: applications to CT organ dosimetry for patients of variable morphometry *Med. Phys.* **35** 2366–82

Mason P A, Hurt W D, Walters T J, D'Andrea J A, Gajsek P, Ryan K L, Nelson D A, Smith K I and Ziriax J M 2000 Effects of frequency, permittivity, and voxel size on predicted specific absorption rate values in biological tissue during electromagnetic-field exposure *IEEE Trans. Microw. Theory Tech.* **48** 2050–8

Neufeld E 2008 High resolution hyperthermia treatment planning *PhD Thesis* no. 17947 Swiss Federal Institute of Technology, Zurich

Neufeld E, Sczcerba D, Chavannes N and Kuster N 2013a A novel medical image databased multiphysics simulation platform for computational life sciences *Interface Focus* **3** 20120058

Neufeld E, Szczerba D and Kuster N 2013b Mechanical simulation-based approach for realistic model shape and posture parametrization *CP'13: 4th Int. Workshop on Computational Phantoms for Radiation Protection, Imaging and Radiotherapy (Zurich, 20–22 May)* pp 14–5

Petoussi-Henss N, Zankl M, Fill U and Regulla D 2002 The GSF family of voxel phantoms *Phys. Med. Biol.* **47** 89–106

Raya S P and Udupa J K 1990 Shape-based interpolation of multidimensional objects *IEEE Trans. Med. Imaging* **9** 32–42

Sato K, Noguchi H, Emoto Y, Koga S and Saito K 2007 Japanese adult male voxel phantom constructed on the basis of CT images *Radiat. Prot. Dosim.* **123** 337–44

Sato K, Noguchi H, Emoto Y, Koga S and Saito K 2009 Development of a Japanese adult female voxel phantom *J. Nucl. Sci. Technol.* **46** 907–13

Schenk A, Prause G and Peitgen H-O 2000 Efficient semiautomatic segmentation of 3D objects in medical images *Medical Image Computing and Computer-Assisted Intervention* (Berlin: Springer) pp 186–95

Schmidt G 2005 *Differential Diagnosis in Ultrasound Imaging: A Teaching Atlas* (Stuttgart: Thieme)

Segars W P and Tsui B 2009 MCAT to XCAT: the evolution of 4D computerized phantoms for imaging research *Proc. IEEE* **97** 1954–68

Sempé M, Pédron G and Roy-Pernot M-P 1979 *Auxologie: méthode et séquences Théraplix* (Paris: Theraplix)

Shephard M S and Georges M K 1991 Automatic three-dimensional mesh generation by the finite Octree technique *Int. J. Numer. Methods Eng.* **32** 709–49

Shewchuk J R 1998 Tetrahedral mesh generation by Delaunay refinement *Proc. 14th ACM Annu. Symp. on Computational Geometry* pp 86–95

Snyder W S, Cook M, Nasset E, Karhausen L, Howells G P and Tipton I 1975 *Report of the Task Group on Reference Man* vol 23 (Oxford: Pergamon)

Spurway J F, Simmons B J and Davies R P 2004 The gallbladder wall: acute cholecystitis versus circumferential gallbladder oedema *ASUM Ultrasound Bull.* **7** 15–16

Stalling D, Westerhoff M and Hege H-C 2005 Amira: a highly interactive system for visual data analysis *The Visualization Handbook* vol 38 (Oxford: Elsevier) pp 749–67

Suri J S, Liu K, Singh S, Laxminarayan S N, Zeng X and Reden L 2002 Shape recovery algorithms using level sets in 2D/3D medical imagery: a state-of-the-art review *IEEE Trans. Inform. Technol. Biomed.* **6** 8–28

Taubin G 1995 Curve and surface smoothing without shrinkage *IEEE Proc. 5th Int. Conf. on Computer Vision* pp 852–7

Tsui B M, Terry J A and Gullberg G T 1993 Evaluation of cardiac cone-beam single photon emission computed tomography using observer performance experiments and receiver operating characteristic analysis *Investigative Radiol.* **28** 1101–12

Udupa J K and Saha P K 2003 Fuzzy connectedness and image segmentation *Proc. IEEE* **91** 1649–69

von Siebenthal M, Székely G, Gamper U, Boesiger P, Lomax A and Cattin P 2007 4D MR imaging of respiratory organ motion and its variability *Phys. Med. Biol.* **52** 1547–64

Xu X, Chao T and Bozkurt Z 2000 VIP-MAN: an image-based whole-body adult male model constructed from color photographs of the visible human project for multi-particle Monte Carlo calculations *Health Phys.* **78** 476–86

Xu X G, Taranenko V, Zhang J and Shi C 2007 A boundary-representation method for designing whole-body radiation dosimetry models: pregnant females at the ends of three gestational periods—RPI-P3, -P6 and -P9 *Phys. Med. Biol.* **52** 7023–44

Zhang B, Ma J, Liu L and Cheng J 2007 CNMAN: a Chinese adult male voxel phantom constructed from color photographs of a visible anatomical data set *Radiat. Prot. Dosim.* **124** 130–6

Zubal I G *et al* 1994 Computerized three-dimensional segmented human anatomy *Med. Phys.* **21** 299–302